Journal of Intelligent Computing and Networking
https://www.ffspub.com/index.php/jicn/index
ISSN 3079-9228 (print)
ISSN 3107-2798 (online)
E-mail: jicn.office@ffspub.com

Article

PRIME: A Privacy-Enhanced Framework for Efficient Unknown Worker Recruitment in Heterogeneous Mobile Crowdsensing

Haozhou Liu, Honglong Chen†, Huansheng Xue, Yongji Sun, Junru Hei, Yudi Guo
College of Control Science and Engineering, China University of Petroleum (East China), Qingdao 266580, China
†*E-mail: chenhl@upc.edu.cn*

Received: April 30, 2026 / Revised: May 23, 2026 / Accepted: June 1, 2026 / Published online: June 8, 2026

Abstract: With the rapid advancement of sensor technologies and ubiquitous mobile intelligence, Mobile Crowdsensing (MCS) has become an effective paradigm for large-scale sensing tasks. It overcomes the limitations of traditional fixed sensing infrastructures while enabling low-cost and flexible data collection. However, practical MCS deployment still faces significant challenges. Conventional privacy-preserving approaches often suffer from high computational overhead or degraded data utility. Most existing recruitment methods assume prior knowledge of worker reliability, rendering them ineffective for unknown workers. Moreover, static task allocation strategies fail to adapt to the heterogeneous and dynamic characteristics of real-world sensing tasks. To address these limitations, we propose PRIME (Privacy-preserving Recruitment and Incentive-driven Multi-task allocation with freshness awareness), a privacy-enhanced framework for efficient unknown worker recruitment in heterogeneous Mobile Crowdsensing. The framework incorporates a lightweight privacy-preserving mechanism based on encoding and masking techniques to ensure both data integrity and secure transmission. In static scenarios, the recruitment process is modeled as a Combinatorial Multi-Armed Bandit (CMAB) problem with a bidirectional arm structure that jointly considers task requirements and worker preferences. A collateral function is introduced to mitigate the risk of malicious data submission. In dynamic scenarios, an optimal task allocation strategy is designed to account for system constraints and heterogeneous worker behaviors, thereby maximizing overall system utility. Extensive experiments on both synthetic and real-world datasets demonstrate that PRIME outperforms state-of-the-art baselines in privacy protection, recruitment effectiveness, and overall system performance.

Keywords: Mobile Crowdsensing; Privacy Protection; Unknown Workers; Collateral Function; Task Allocation
https://doi.org/10.64509/jicn.22.106

1 Introduction

With the rapid development of sensor technologies and smart mobile devices [1, 2], portable intelligent devices have become indispensable in daily life. These devices enable individuals to collect multimodal data, thereby accelerating the advancement of Mobile Crowdsensing (MCS). Unlike conventional static sensor networks that require extensive prior deployment, MCS harnesses a large, naturally distributed population of mobile workers to fulfill sensing tasks. This paradigm offers low deployment cost, real-time sensing capability, wide coverage, and high efficiency, and has found broad applications in environmental monitoring [3], smart cities [4], traffic planning [5], and social recommendation [6].

A typical MCS system comprises three entities: task requesters, the crowdsensing platform, and mobile workers. Task requesters publish sensing tasks via a cloud-based platform, which assigns them to suitable workers. Workers then perform the tasks, upload collected data in return for rewards, and the platform delivers the aggregated results to the requesters [7]. As the scale of workers and tasks expands, interactions among these entities risk exposing sensitive information, raising significant privacy concerns. Consequently, privacy-preserving task allocation has emerged as a critical challenge in MCS [8].

Task requesters demand high-quality sensing data, yet worker quality is inherently heterogeneous and may vary across tasks. Moreover, the collection, transmission, and

† Corresponding author: Honglong Chen
*Academic Editor: Xiuli Bi

processing of user data can inadvertently reveal sensitive attributes such as location and behavioral patterns. Although privacy-preserving mechanisms mitigate these risks through encoding and masking prior to upload, they complicate worker evaluation and recruitment [9]. To tackle this issue, Multi-Armed Bandit (MAB) models have been increasingly employed for online worker quality learning and adaptive recruitment under uncertainty [10–12]. These approaches balance exploration of new workers with exploitation of known ones, thereby improving long-term sensing quality while reducing regret from suboptimal decisions.

In addition to data quality, task timeliness plays a pivotal role in many MCS applications, such as traffic monitoring and environmental assessment, where strict deadlines apply. The Age of Information (AoI) metric has thus been introduced to quantify information freshness [13, 14]. Integrating AoI into worker evaluation and task allocation enhances task freshness, completion efficiency, and resource utilization.

Despite these advances, a notable gap persists between static learning and dynamic allocation. Privacy-preserving recruitment, quality-aware learning, freshness-aware scheduling, and incentive mechanisms are frequently investigated in isolation. Few studies have examined how knowledge accumulated from privacy-preserving static scenarios can be effectively transferred to dynamic multi-task allocation while simultaneously addressing freshness requirements, worker preferences, and budgeted incentivess [15]. In practice, however, MCS platforms must progressively learn worker characteristics under privacy constraints in static settings and subsequently leverage this knowledge for robust allocation in dynamic environments.

This paper studies the problem of task allocation from the perspective of worker interactions in both static and dynamic scenarios. It proposes PRIME (Privacy-preserving Recruitment and Incentive-driven Multi-task allocation with freshness awareness), a unified framework that integrates privacy-preserving evaluation, quality-aware and AoI-aware learning, bidirectional preference learning, and incentive design. In static scenarios, the platform employs an MAB-based recruitment mechanism to continuously learn worker quality and information freshness, gradually converting unknown workers into known ones. A collateral-based penalty mechanism further enhances recruitment reliability by discouraging infeasible or malicious behavior under coverage, capacity, and budget constraints. In dynamic scenarios, the accumulated knowledge guides proactive sensing and reverse-auction-based task allocation amid multi-task competition. Overall, PRIME improves system utility, stabilizes recruitment through progressive learning, and fosters cost-effective, preference-consistent participation in dynamic MCS environments.

The main contributions of this paper are as follows:

- We design a Spatial Generalization-based Double-sided Cryptographic Encryption for Candidate Selection (SG-DCE) mechanism for bilateral location privacy-preserving worker evaluation and candidate filtering. By encoding raw locations into privacy-preserving grid representations, the platform estimates spatial relevance without accessing sensitive location data directly.
- We propose a quality-aware and AoI-aware online recruitment mechanism with bidirectional preference learning. A Combinatorial Multi-Armed Bandit (CMAB)-based process explores new workers and exploits known workers under privacy protection, while worker preferences are adaptively updated via bidding feedback to enhance recruitment robustness and matching accuracy.
- We formulate dynamic task allocation as a system utility maximization problem under coverage, capacity, and budget constraints, and develop a genetic-algorithm-based reverse auction with a critical-pricing-inspired payment rule to enable cost-effective and truthful participation.

The remainder of this paper is organized as follows. Section 2 reviews related work. Section 3 presents the system overview, introduces the system models, and formulates the system utility maximization problem. Section 4 details the proposed PRIME framework, including privacy-preserving candidate filtering, quality-aware and AoI-aware secure recruitment, and dynamic task allocation with proactive mobility guidance. Section 5 reports simulation settings and performance evaluation results. Finally, Section 6 concludes the paper and discusses future research directions.

2 Related Work

2.1 Location Privacy Preservation

Location privacy preservation constitutes a core challenge in MCS, as worker selection and task assignment inherently depend on spatial information that may disclose sensitive attributes. Existing studies primarily address this issue from two perspectives.

One line of research focuses on privacy-preserving recruitment and assignment. Zhao *et al.* [8] formulated privacy-preserving task assignment as a bi-objective optimization problem that balances system utility and privacy leakage. Tang *et al.* [12] proposed a bilateral location privacy-preserving scheme integrated with quality-aware worker recruitment.

Another line incorporates privacy mechanisms into subsequent crowdsensing stages, such as secure data collection and truth discovery. Representative works include Liu *et al.* [16] on Secure CrowdSourcing, Zhu *et al.* [17] on trustworthy data collection, and Bai *et al.* [18] on privacy-aware truth discovery.

Despite these efforts, most studies treat privacy-preserving recruitment and downstream data processing in isolation. The influence of protected location representations on candidate filtering, adaptive recruitment, and subsequent task allocation remains underexplored. A key challenge thus lies in designing location privacy mechanisms that effectively conceal raw coordinates while still supporting efficient worker screening and decision-making under uncertainty.

2.2 Multi-Armed Bandit-Based Learning for Crowdsensing

To handle uncertainty in worker quality and dynamic system conditions, learning-based approaches have gained traction in

MCS. Reinforcement learning (RL) has been applied to dynamic task allocation and participant selection by modeling sequential decisions and long-term system dynamics [19–21]. However, RL methods typically incur substantial training costs and computational overhead, which limits their applicability in large-scale and latency-sensitive scenarios.

In comparison, MAB models provide a lightweight alternative by balancing exploration and exploitation with limited feedback. Such models are particularly suitable for online worker recruitment and task assignment. For instance, Wang *et al.* [10] employed combinatorial MAB for truthful worker recruitment, while Song *et al.* [22] developed a two-stage MAB framework for joint task selection and recruitment. An *et al.* [11] investigated privacy-preserving recruitment with sensing quality evaluation, and Tang *et al.* [12] integrated bilateral location privacy into quality-aware service construction. Ouyang *et al.* [23] further extended MAB-based recruitment by incorporating worker reliability and strategic interactions.

Nevertheless, the majority of MAB-based studies emphasize reward maximization, recruitment efficiency, or overall system utility. Limited attention has been paid to worker-side preference heterogeneity and its impact on participation behavior and allocation quality. In practice, workers exhibit diverse preferences regarding task types, locations, and workloads, which critically influence their willingness to participate and sensing performance. Overlooking these factors can result in inefficient recruitment, especially when worker profiles are progressively learned under privacy constraints and later exploited in dynamic allocation.

2.3 Task Assignment

Task assignment lies at the heart of Mobile Crowdsensing, aiming to match tasks with suitable workers so as to maximize system utility under constraints on budget, coverage, and timeliness. Early studies modeled the problem as combinatorial optimization tasks and solved them via greedy heuristics, flow-based methods, or approximation algorithms. Examples include Xiao *et al.* [24] developed mobility-aware offline and online assignment algorithms in mobile social networks, and Hu *et al.* [25] proposed a greedy approximation for QoS-sensitive task assignment.

Subsequent research incorporated richer objectives, including coverage, sensing quality, worker heterogeneity, and hybrid participation modes. Wang *et al.* [26] introduced a two-phase framework jointly optimizing opportunistic and participatory workers under a unified budget. Liu *et al.* [27] examined hybrid user-based task assignment under delay-sensitive conditions with heterogeneous worker qualities.

More recent efforts have explored dynamic matching, freshness awareness, and incentive mechanisms. These include matching-based service trading, stagewise stable matching for spatial-temporal tasks, reverse-auction-based truthful incentives, utility-optimal online pricing, as well as AoI-aware incentive design [13, 28–32]. Such advances have significantly improved both assignment efficiency and adaptability in dynamic environments.

However, existing task assignment approaches still largely address privacy protection, worker learning, preference modeling, and dynamic allocation in isolation. In realistic MCS scenarios, effective assignment requires jointly considering location suitability, sensing quality, information freshness, worker preferences, and budget-constrained incentives. In particular, few studies have examined how knowledge progressively accumulated from privacy-preserving static scenarios can be transferred to dynamic multi-task allocation. This motivates the need for a unified framework that seamlessly connects privacy-preserving worker evaluation, online learning, preference-aware recruitment, and dynamic task allocation under heterogeneous constraints.

3 System Overview and Problem Formulation

The task allocation problem is formulated after first outlining the key components and operational principles of the privacy-preserving vehicular mobile crowdsensing system. In addition to the conventional task, worker, and platform models, the AoI is incorporated to account for the freshness requirements and delay sensitivity of sensing tasks.

3.1 System Overview

This work considers a vehicular mobile crowdsensing platform that exploits the distributed sensing capabilities of vehicles for large-scale traffic-related data collection. Task requesters publish sensing tasks, workers participate in tasks of interest and receive rewards upon successful completion, and the platform manages worker recruitment and task allocation.

The platform operates in discrete rounds. Each round consists of four stages: region partitioning, information acquisition, task allocation, and task execution. First, the sensing area is divided into fine-grained spatial grids. During the information acquisition stage, each worker uploads the required information and selects one grid based on personal preference and available time budget. Because grids are spatially separated and each round has limited execution time, a worker can select only one grid per round. Newly arrived workers register at this stage. Any tasks or workers that arrive during the current round are deferred to the task allocation stage of the next round. In the task execution stage, selected workers carry out their assigned tasks and upload the collected data. Tasks that remain unfinished are carried over to later rounds.

For modeling tractability, the following assumptions are made. Tasks within the same grid are geographically proximate, rendering intra-grid travel overhead negligible relative to the dominant mobility cost of reaching the assigned region. Each worker selects only one grid and specifies a time budget for task execution within that region. Workers are assumed to be rational and self-interested; consequently, they may reject tasks whose effort exceeds their time budget or whose reward is insufficient. Under these assumptions, this study focuses on efficient worker recruitment, task allocation, and scheduling within individual grids.

Two sensing modes are distinguished: static and dynamic. In the static mode (e.g., when vehicles are temporarily

stationary at traffic lights or congestion points), workers perform relatively low-urgency tasks. This enables the platform to progressively learn worker quality and preferences under privacy constraints. In the dynamic mode, the platform leverages the accumulated knowledge to adaptively allocate tasks according to real-time traffic conditions, task freshness requirements, and mobility constraints. As illustrated in Figure 1, the round-based workflow provides the foundation for the task model, worker model, platform model, and utility-maximization formulation.

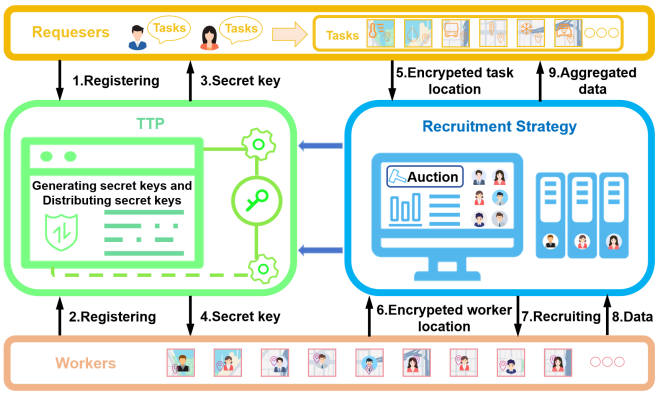

Figure 1: The system workflow of the MCS platform

This paper addresses a privacy-constrained task allocation problem in vehicular participatory sensing. Vehicles act as mobile sensing workers that actively engage in data collection via the platform. The system operates in a dynamic traffic environment in which vehicle states (moving or stationary), energy budgets, and worker preferences evolve over time. The platform must therefore make online allocation decisions under incomplete information.

The system consists of three types of entities. The heterogeneous task, heterogeneous worker, and privacy-preserving platform models are defined as follows.

Definition 1 (Heterogeneous Task) A task requester submits a set of heterogeneous tasks $\mathscr{T} = \{t_1, t_2, \ldots, t_N\}$, where N is the number of tasks. Each task t_j is characterized by the tuple $t_j = \{l_{t_j}, s_{t_j}, DB_j, q_j, A_j\}$, where l_{t_j} denotes the task location, s_{t_j} the required sensing capability set, DB_j the required data volume, q_j the number of divisible subtasks, and A_j the Age of Information (AoI) threshold.

Definition 2 (Heterogeneous Worker) Consider a set of M heterogeneous workers $\mathscr{U} = \{u_1, u_2, \ldots, u_M\}$. Each worker u_i is characterized by the tuple $u_i = \{mv_i, sv_i, l_{u_i}, E_i, s_i^u, \Gamma_i, m_i\}$, where mv_i is the moving speed, sv_i the per-unit-time data sensing/processing rate, l_{u_i} the initial location, E_i the energy budget, s_i^u the number of sensing capabilities, Γ_i the time budget, and m_i the sensing quality. Because worker quality is initially unknown, m_i is modeled as a random variable $m_i \sim \mathscr{N}(\mu_m, \sigma_m^2)$ and is refined online based on feedback from completed tasks.

Definition 3 (Privacy-Preserving Platform Model) The platform allocates sensing tasks to suitable workers under a limited budget Φ. To prevent information leakage, privacy-preserving mechanisms (e.g., encryption and secure multi-party computation) protect both task and worker information during bidding, candidate filtering, and task allocation.

3.2 Problem Formulation

Based on the models above, the task allocation problem is formulated as the maximization of system utility in a privacy-preserving vehicular crowdsensing environment. The main variables and parameters used in the following formulation are summarized in Table 1. Task execution by each worker incurs mobility cost, sensing time, and energy consumption. The platform aims to maximize overall system utility by balancing sensing quality, task timeliness, and economic cost, subject to constraints on worker time and energy budgets, task capacity, and platform budget.

Table 1: Key Notations

Symbol	Description
$\mathscr{T}, N$	Set and number of tasks
$\mathscr{U}, M$	Set and number of workers
l_{t_j}	Location of task t_j
l_{u_i}	Location of worker u_i
s_{t_j}	Required sensing capability of task t_j
s_i^u	Available sensing capability of worker u_i
DB_j	Required data volume of task t_j
q_j	Number of subtasks of task t_j
A_j	AoI threshold of task t_j
mv_i	Moving speed of worker u_i
sv_i	Data sensing/processing rate of worker u_i
E_i, Γ_i	Energy and time budgets of worker u_i
m_i	True sensing quality of worker u_i
$d_{i,j,k}$	Distance between worker u_i and subtask (j,k)
$\theta_{i,j,k}^{\text{move}}$	Movement time of worker u_i to subtask (j,k)
$\theta_{i,j,k}^{\text{sen}}$	Sensing time of worker u_i for subtask (j,k)
$\theta_{i,j,k}^{\text{exe}}$	Total execution time of worker u_i for subtask (j,k)
$D_{i,j,k}$	Collected data volume for subtask (j,k)
$e_{i,j,k}^{\text{move}}$	Movement energy consumption
$e_{i,j,k}^{\text{sen}}$	Sensing energy consumption
$te_{i,j,k}$	Total energy consumption
$A_{i,j,k}$	Realized AoI for subtask (j,k), including delay
Cost_{u_i}	Participation cost of worker u_i
V_i^u, V_j^t	Utility of worker u_i and requester of task t_j
V	Overall system utility
$x_{i,j,k}$	Binary assignment variable
Φ	Platform budget
$p_{i,j,k}$	Payment for assigning subtask (j,k) to worker u_i

3.2.1 User Mobility Model

The mobility distance between worker u_i and a subtask location is

$$d_{i,j,k} = \sqrt{\left(l_i^{\text{lat}} - l_j^{\text{lat}}\right)^2 + \left(l_i^{\text{lon}} - l_j^{\text{lon}}\right)^2}. \tag{1}$$

The corresponding travel time is

$$\theta_{i,j,k}^{\text{move}} = \frac{d_{i,j,k}}{mv_i}. \tag{2}$$

The energy consumed during movement is given by

$$e_{i,j,k}^{\text{move}} = \alpha_i \cdot d_{i,j,k}, \tag{3}$$

where α_i denotes the per-unit-distance energy coefficient for worker u_i.

3.2.2 Data Sensing Model

Workers collect data using onboard sensors with heterogeneous sensing rates sv_i. The collected data volume and sensing energy consumption are

$$\begin{aligned} D_{i,j,k} &= \theta^{\text{sen}}_{i,j,k} \cdot sv_i, \\ e^{\text{sen}}_{i,j,k} &= \beta_i \cdot D_{i,j,k}. \end{aligned} \tag{4}$$

where β_i is the per-unit-data energy coefficient for worker u_i.

3.2.3 Time and Energy Consumption Model

The total execution time and energy consumption for worker u_i on subtask (j,k) are

$$\begin{aligned} \theta^{\text{exe}}_{i,j,k} &= \theta^{\text{move}}_{i,j,k} + \theta^{\text{sen}}_{i,j,k}, \\ te_{i,j,k} &= e^{\text{move}}_{i,j,k} + e^{\text{sen}}_{i,j,k}. \end{aligned} \tag{5}$$

3.2.4 Age of Information Model

The AoI for a subtask is modeled as

$$A_{i,j,k} = A_0 K_{i,j,k} + \frac{1}{2} K^2_{i,j,k}, \tag{6}$$

where $K_{i,j,k}$ denotes the delay experienced by the subtask.

3.2.5 Utility Model

To encourage reliable participation in the reverse auction process, a collateral-aware incentive mechanism is introduced. Specifically, each worker u_i voluntarily commits a pledged collateral amount denoted by s^0_{iu}, while $\max\{s^t_j\}$ represents the maximum allowable collateral associated with task t_j.

Accordingly, the normalized collateral ratio is defined as

$$\rho_{ij} = \frac{s^0_{iu}}{\max\{s^t_j\}}, \tag{7}$$

A larger collateral ratio indicates stronger participation willingness and higher execution confidence from worker u_i.

Based on the above mechanism, the effective worker cost is modeled as

$$\text{Cost}_{u_i} = k_c \left(1 + \log_{10}(r_i) - \lambda \log(1+\rho_{ij})\right), \tag{8}$$

where $\lambda > 0$ is a weighting factor controlling the influence of the collateral incentive mechanism.

$$V^u_i = \begin{cases} p_{i,\tau} - \text{Cost}_{u_i}, & u_i \in \mathscr{S}_\tau, \\ 0, & u_i \notin \mathscr{S}_\tau. \end{cases} \tag{9}$$

where $\mathscr{S}_\tau \subseteq \mathscr{U}$ denotes the set of selected workers in recruitment round τ, and $p_{i,\tau}$ is the payment received by worker u_i in that round.

The requester utility is

$$V^t_j = \sum_{i \in S'} (m_i - p_i). \tag{10}$$

The overall system utility is

$$V = V_u + V_t. \tag{11}$$

3.2.6 Optimization Problem

Let $\mathbf{X} = \{x_{i,j,k}\}$ denote the binary assignment variables. The optimization problem, referred to as the Privacy-preserving Heterogeneous and Efficient Crowdsensing Selection (PHECS) problem, is formulated as

$$\mathbf{P1}: \max \quad V(\mathbf{X}) = V_u(\mathbf{X}) + V_t(\mathbf{X}),$$
$$\text{s.t.} \quad \begin{cases} \sum\limits_i x_{i,j,k} \le q_j, & \forall j,k, \\ \sum\limits_{j,k} x_{i,j,k}\, \theta^{\text{exe}}_{i,j,k} \le \Gamma_i, & \forall i, \\ \sum\limits_{j,k} x_{i,j,k}\, te_{i,j,k} \le E_i, & \forall i, \\ \sum\limits_{i,j,k} x_{i,j,k}\, p_{i,j,k} \le \Phi, & \\ \sum\limits_{i,k} x_{i,j,k} A_{i,j,k} \le A_j, & \forall j, \\ x_{i,j,k} \in \{0,1\}, & \forall i,j,k. \end{cases} \tag{12}$$

Due to the binary assignment variables and the presence of multiple coupled resource constraints, the proposed PHECS problem belongs to the class of combinatorial optimization problems. Solving **P1** to optimality is therefore non-trivial. To formally characterize its computational complexity, we establish the NP-hardness of the PHECS problem in the following theorem.

Theorem 1 *The PHECS problem is NP-hard.*

Proof We prove the NP-hardness of the PHECS problem by a polynomial-time reduction from the two-dimensional knapsack problem (2D-KP), which is known to be NP-hard.

Consider an arbitrary instance of the 2D-KP consisting of a finite set of items $\mathscr{I}$, where each item $m \in \mathscr{I}$ is associated with a profit p_m and two resource consumption coefficients w^1_m and w^2_m, together with two knapsack capacities W^1 and W^2. We construct a special instance of the PHECS problem as follows:

- Each feasible assignment triple (i,j,k) with $x_{i,j,k} \in \{0,1\}$ in PHECS corresponds to one item m in the 2D-KP.
- The marginal contribution to the objective, i.e., the increase in $V(\mathbf{X}) = V_u(\mathbf{X}) + V_t(\mathbf{X})$ when setting $x_{i,j,k} = 1$, is mapped to the profit p_m of the item.
- The time consumption $tt_{i,j,k}$ and energy consumption $te_{i,j,k}$ correspond to the two resource consumption dimensions w^1_m and w^2_m.
- For each worker i, the time budget Γ_i and energy budget E_i directly serve as the two knapsack capacities W^1 and W^2.

Under this reduction, a feasible solution $\mathbf{X}$ to the PHECS instance corresponds to a feasible 2D-KP packing with equal objective value, and vice versa. Since 2D-KP is NP-hard, the restricted PHECS problem is NP-hard. The full PHECS problem adds further constraints, making it at least as hard. Therefore, the PHECS problem is NP-hard. □

4 The Design of the PRIME Framework

4.1 Overview of the PRIME Framework

The PHECS problem is proven NP-hard via reduction from the 2D-KP (Theorem 1), rendering exact optimization computationally intractable at scale. Joint enforcement of worker

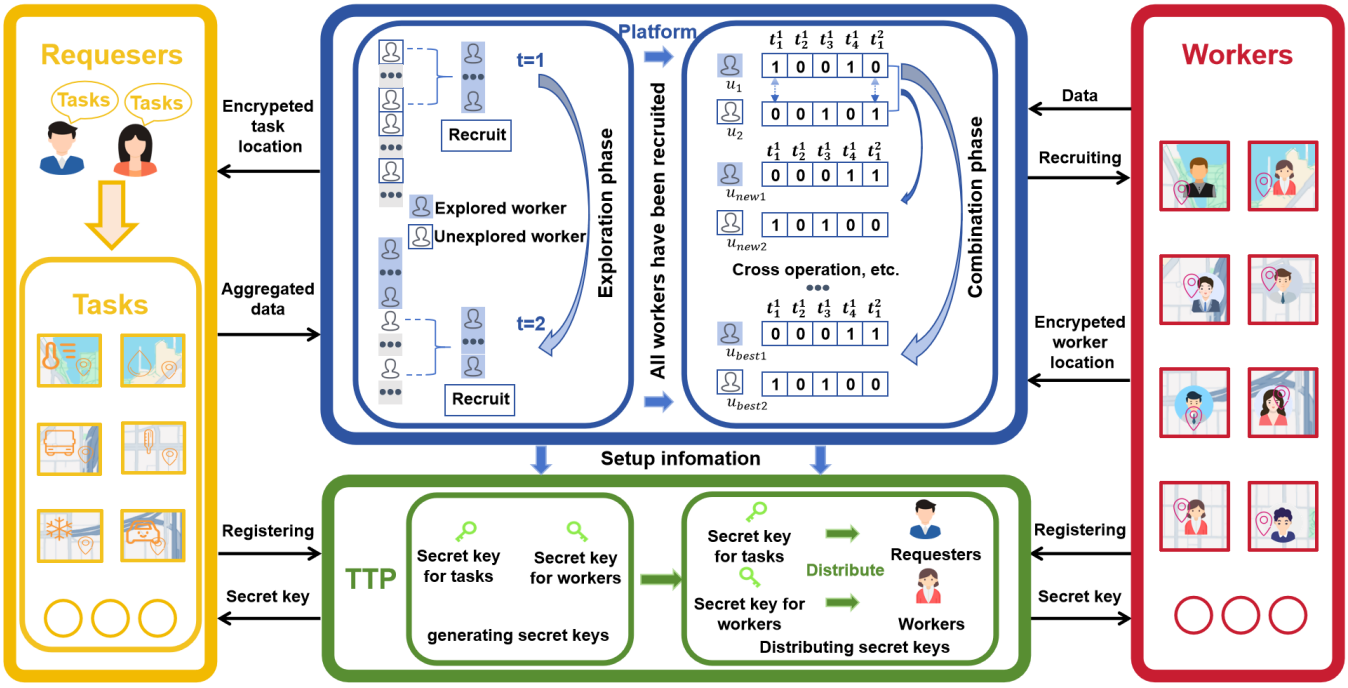

Figure 2: The detailed process of our proposed PRIME scheme.

resource budgets, platform cost constraints, task capacity limits, and AoI thresholds further precludes any polynomial-time exact solution. This intractability motivates the design of an efficient approximation framework.

To this end, we propose PRIME, which jointly addresses: location privacy protection, online learning of unknown worker reliability, bidirectional preference modeling, and long-term system utility maximization under resource and freshness constraints.

As illustrated in Figure 2, PRIME involves four principal entities: the crowdsensing platform, task requesters, mobile workers, and a trusted third party (TTP). The TTP is responsible for system initialization, including identity registration and cryptographic key distribution, thereby establishing a secure foundation for all subsequent privacy-preserving operations. Following initialization, the platform executes all recruitment and allocation decisions without accessing raw location data or sensitive worker preferences.

The PRIME framework operates through three tightly coupled procedures.

Privacy-preserving evaluation and candidate selection. Under bilateral location privacy constraints, the platform employs the SG-DCE (Spatial Generalization-based Double-sided Cryptographic Encryption for Candidate Selection) mechanism to estimate worker spatial relevance and sensing capability using only anonymized grid representations. Raw location coordinates and preference data remain inaccessible.

Quality-aware and AoI-aware online recruitment with bidirectional preference learning. Worker quality and AoI contribution are modeled as unknown parameters and estimated online via a MAB framework, with each worker as an arm. At each recruitment epoch, the Unknown-worker UCB Estimation (UUE-UCB) mechanism strategy balances estimated quality and an exploration bonus. Bidirectional preference learning then updates both platform-side worker evaluations and worker-side task preferences from bidding feedback. AoI enters the reward signal to penalize stale contributions.

Feedback-driven task allocation and incentive optimization. Given the learned profiles from Procedure 2, the platform solves the task allocation subproblem via the Two-Stage Greedy Algorithm (TSGA). TSGA runs in polynomial time and yields an approximate optimal assignment subject to constraints on mobility distance, travel time, data sensing and energy models, total time and energy consumption, participation cost, worker utility, requester utility, system utility, Age-of-Information, coverage, capacity, and budget. A reverse auction determines incentive payments. Upon task completion, sensing quality and AoI feedback return to UCB to update estimates and preferences, closing the loop.

Collectively, these three procedures form a closed-loop system: the first procedure filters the feasible worker set under strict privacy constraints, the second procedure learns worker quality and preferences under uncertainty, and the third procedure performs efficient task allocation while feeding back observations for continuous improvement. This design seamlessly integrates bilateral location privacy preservation, online learning under uncertainty, and freshness-aware incentives within a unified optimization framework.

4.2 Privacy-Preserving Evaluation and Candidate Selection

Under bilateral location privacy constraints, neither the platform nor the workers are willing to disclose their exact spatial coordinates. Consequently, the platform cannot directly compute the Euclidean distance $d_{i,j,k}$ between worker u_i and subtask $s_{j,k}$. To address this challenge, we propose a SG-DCE mechanism,which maps continuous spatial locations into a privacy-preserving discrete domain while retaining proximity information.

Specifically, a trusted third party (TTP) initializes a global spatial grid with resolution Δ and reference point (B_0, L_0).

Each location is discretized into a grid index as

$$(i,j) = \left(\left\lfloor \frac{\text{lon} - L_0}{\Delta_{\text{lon}}} \right\rfloor, \left\lfloor \frac{\text{lat} - B_0}{\Delta_{\text{lat}}} \right\rfloor \right), \tag{13}$$

where (i,j) denotes the corresponding grid cell. This discretization reduces spatial precision and prevents exact location reconstruction.

To further enhance privacy, the grid indices are transformed into obfuscated identifiers via Base32 encoding:

$$\text{cell\_id} = \text{Base32}(i) \parallel \text{Base32}(j). \tag{14}$$

The resulting cell_id reveals only coarse-grained spatial information and is resistant to direct inversion without knowledge of the grid parameters.

Although the above mapping is deterministic, it inherently preserves spatial locality, i.e., geographically close locations are more likely to fall into the same or neighboring grid cells. To facilitate theoretical analysis, we approximate this locality-preserving behavior using the p-stable locality-sensitive hashing (LSH) framework. Accordingly, the probability that two locations with distance $d_{i,j,k}$ are mapped to the same grid cell can be expressed as

$$P(d_{i,j,k}) = \int_0^{\Delta} \frac{1}{d_{i,j,k}} f_p\left(\frac{t}{d_{i,j,k}}\right)\left(1 - \frac{t}{\Delta}\right) dt, \tag{15}$$

where $f_p(\cdot)$ denotes the probability density function of the p-stable distribution.

Based on this probabilistic characterization, we quantify the privacy leakage by relating the mechanism to (ε, δ)-differential privacy. In particular, the distinguishability between two neighboring locations differing by δ_{dist} is bounded as

$$\varepsilon \geq \ln\left(\frac{P(d_{i,j,k})}{P(d_{i,j,k} + \delta_{dist})}\right), \tag{16}$$

which captures the worst-case privacy leakage induced by the grid mapping.

To enable secure candidate matching, each worker generates a cryptographic token using a keyed hash function:

$$\text{token}_i = \text{HMAC}_K(\text{dom\_id} \parallel \text{cell\_id}_i), \tag{17}$$

where K is a secret key known only to the TTP. The use of HMAC ensures collision resistance and prevents adversaries from inferring the underlying location or linking tokens across domains.

Given the token set $\mathscr{T}_{j,k}$ associated with subtask $s_{j,k}$, the platform constructs the candidate worker set as

$$\mathscr{U}_{cand} = \{u_i \mid \text{token}_i \in \mathscr{T}_{j,k}\}. \tag{18}$$

In this way, the platform can perform proximity-based candidate filtering without accessing raw location data. The proposed SG-DCE mechanism thus achieves a balance between privacy protection and spatial selectivity, providing a secure foundation for subsequent quality-aware and AoI-aware task allocation.

Algorithm 1 summarizes the SG-DCE procedure. First, the worker locally computes and encrypts its grid identifier into a secure HMAC token before uploading (lines 1–3). Next, for each subtask, the platform expands the neighborhood around the task center grid and generates the corresponding query token set (lines 6–11). Finally, the platform performs blind matching to identify valid candidates without accessing raw coordinates or precise distances (lines 12–13). This design converts continuous spatial proximity checks into discrete token matching, thereby preserving location privacy during candidate selection while maintaining practical utility for downstream recruitment and allocation.

The complexity of SG-DCE is calculated as follows. Token generation for n workers takes $O(n)$ time, as location mapping and HMAC computations are $O(1)$ operations. Generating the candidate token set involves $O(R_{\text{grid}}^2)$ neighboring cells within radius R_{grid}. Candidate selection via a hash set takes an additional $O(n)$. Therefore, summing these operations, the total complexity of SG-DCE simplifies to $O(n + R_{\text{grid}}^2)$.

Algorithm 1 SG-DCE: Spatial Generalization-based Double-sided Cryptographic Encryption for Candidate Selection

Require: Worker u_i private location (lat_i, lon_i), task sub-location (lat_j, lon_j), grid $(B_0, L_0, \Delta_{\text{lon}}, \Delta_{\text{lat}})$, dom_id, key K, radius r

Ensure: Candidate set $\mathscr{U}_{\text{cand}}$

1: $\text{cell\_id}_i \leftarrow \text{Base32}\left(\left\lfloor \frac{\text{lon}_i - L_0}{\Delta_{\text{lon}}} \right\rfloor\right) \parallel \text{Base32}\left(\left\lfloor \frac{\text{lat}_i - B_0}{\Delta_{\text{lat}}} \right\rfloor\right)$
2: $token_i \leftarrow \text{HMAC}_K(dom\_id \parallel cell\_id_i)$
3: Upload $token_i$ to platform
4: Compute (gx_j, gy_j) by same grid mapping
5: $R_{grid} \leftarrow \lceil r / \min(\Delta_{\text{lon}}, \Delta_{\text{lat}}) \rceil$
6: $\mathscr{T}_{j,k} \leftarrow \emptyset$
7: **for** each grid cell (x,y) within R_{grid} of (gx_j, gy_j) **do**
8: $\quad cell\_id_{xy} \leftarrow \text{Base32}(x) \parallel \text{Base32}(y)$
9: $\quad token_{xy} \leftarrow \text{HMAC}_K(dom\_id \parallel cell\_id_{xy})$
10: $\quad \mathscr{T}_{j,k} \leftarrow \mathscr{T}_{j,k} \cup \{token_{xy}\}$
11: **end for**
12: $\mathscr{U}_{\text{cand}} \leftarrow \{u_i \mid token_i \in \mathscr{T}_{j,k}\}$
13: **return** $\mathscr{U}_{\text{cand}}$

4.3 Quality-aware and AoI-aware Online Recruitment with Bidirectional Preference Learning

Following the privacy-preserving evaluation and candidate selection stage, which yields a set of spatially eligible workers, the platform proceeds to online recruitment under uncertainty. To address unknown worker quality while preserving bilateral location privacy, we formulate the problem as a CMAB and propose the UUE-UCB mechanism. The objective is to progressively maximize long-term system utility by learning worker reliability online, striking a balance between exploration and exploitation.

Exploitation Component: For workers with sufficient historical observations, the exploitation utility is defined as

$$U_\tau = \sum_{u_i \in \mathscr{S}_\tau^{\text{kn}}} \left[\omega_3 m_i + \omega_4 \left(1 - \frac{\bar{A}_{i,\tau}}{A_{\max}}\right)\right], \tag{19}$$

where $\bar{A}_{i,\tau}$ denotes the average AoI incurred by worker u_i up to round τ.

Exploration Component: For workers lacking sufficient observations, the exploration utility is defined as

$$X_\tau = \sum_{u_i \in \mathscr{S}_\tau^{\text{ukn}}} \left[\omega_1 \left(1 - \frac{\tilde{d}_{i,\tau}}{d_{\max}}\right) + \omega_2 \left(1 - \frac{b_{i,\tau}}{b_{\max}}\right) \right], \quad (20)$$

where $\tilde{d}_{i,\tau}$ is the privacy-preserving distance indicator and $b_{i,\tau}$ is the bid in round τ.

The overall utility in round τ is a weighted combination of U_τ and X_τ, capturing the trade-off between reliability and exploration.

UCB-based Strategy Selection: The platform maintains a set of strategy arms $\mathscr{A} = \{a_1, \ldots, a_Z\}$, each corresponding to a weight vector $(\omega_1, \omega_2, \omega_3, \omega_4)$. At each recruitment round τ, the arm is selected via

$$z_{\tau+1} = \arg\max_{a_z \in \mathscr{A}} \left(\bar{\mu}_z(\tau) + \sqrt{\frac{2\ln \tau}{N_z(\tau)}} \right), \quad (21)$$

where $\bar{\mu}_z(\tau)$ and $N_z(\tau)$ denote the empirical reward and pull count of arm a_z up to round τ, respectively.

Dynamic Incentive Mechanism: To encourage long-term participation, the adjusted bid is

$$b'_{i,\tau} = b_{i,\tau}\left(1 - \kappa_{i,\tau} \cdot \mathbb{I}(\tau > \tau_{\text{mid}})\right), \quad (22)$$

with

$$\kappa_{i,\tau} = \min\left(\kappa_{\text{base}} \cdot \frac{N_{i,\tau}^{\text{success}}}{N_{i,\tau}^{\text{total}}}, \kappa_{\max} \right). \quad (23)$$

Deposit Update: The security deposit evolves as

$$\psi_{i,\tau+1} = \min\left(\psi_{i,\tau} + \Delta\psi \cdot \text{sign}(m_i - \mu_m), \psi_{\max}\right). \quad (24)$$

Preference Learning: Worker preference is updated as

$$P_{i,\tau+1}(c) = (1-\eta)P_{i,\tau}(c) + \eta \cdot \frac{N_{i,\tau}(c)}{\sum_{c' \in \mathscr{C}_{i,\tau}^{\text{cand}}} N_{i,\tau}(c')}, \quad c \in \mathscr{C}_{i,\tau}^{\text{cand}}. \quad (25)$$

where c denotes a task type, $\mathscr{C}_{i,\tau}^{\text{cand}} \subseteq \mathscr{C}$ is the set of candidate task types available to worker u_i in round τ, and $N_{i,\tau}(c)$ denotes the number of times worker u_i has participated in or bid for tasks of type c up to round τ.

The proposed UUE-UCB mechanism unifies UCB-based exploration–exploitation, dynamic incentive adjustment, and adaptive preference learning into an online recruitment process. This approach progressively improves the selection of reliable workers while maintaining the privacy–utility trade-off established.

Algorithm 2 summarizes the UUE-UCB-based secure recruitment process. First, the platform selects the optimal strategy arm via the UUE-UCB rule to balance exploitation and exploration (lines 1–2). Next, it performs privacy-preserving recruitment through a reverse auction, adjusting bids according to worker reliability and computing matching scores under the selected weights (lines 3–8). Then, Benford's Law is applied for forgery detection; significant deviations trigger UAV verification and potential deposit forfeiture (lines 9–14), where μ_{UAV} denotes the deviation threshold for triggering UAV verification. Finally, worker profiles, preference beliefs, bid factors, deposits, and MAB parameters are updated based on task outcomes (lines 15–18). Notably, the dynamic deposit adjustment progressively increases $\psi_{i,\tau+1}$ for workers with above-average sensing quality, which raises their selection probability in future rounds by signaling stronger commitment and lowering their effective cost in the auction.

The complexity of UUE-UCB-based secure recruitment depends on several per-round operations. Arm selection among Z arms takes $O(Z)$. Matching n workers to S subtasks using SG-DCE distances dominates each round, requiring $O(S \cdot n \cdot R_{\text{grid}}^2)$. Other linear operations, such as payment computation, Benford detection, and parameter updates, take $O(n)$. Over T_r recruitment rounds, the dominant matching step yields a final UUE-UCB complexity of $O(T_r \cdot S \cdot n \cdot R_{\text{grid}}^2)$.

Algorithm 2 UUE-UCB-Based Secure Recruitment Mechanism

Require: Arms $\mathscr{A}$, privacy-preserving distance $\tilde{d}_{i,j,k}$ via SG-DCE, learning rate η, UAV verification threshold μ_{UAV}, maximum deposit $\psi_{\text{deposit,max}}$

Ensure: $\mathscr{S}_{\text{win}}$, updated $\bar{\mu}_z, N_z$, adjusted bids $b'_{i,j,k}$, deposits ψ_i

1: **for** $\tau = 1$ to T_r **do**
2: Compute UCB for each $a_z \in \mathscr{A}$; select $a_{z_\tau} = (\omega_1, \omega_2, \omega_3, \omega_4)$
3: **for** each subtask $s_{j,k}$ and $u_i \in \mathscr{U}_{\text{cand}}$ **do**
4: Get $\tilde{d}_{i,j,k}$ via SG-DCE
5: $b'_{i,j,k} \leftarrow b_{i,j,k}(1 - \kappa_{i,\tau} \cdot \mathbb{I}(\tau > \tau_{\text{mid}}))$
6: Compute matching score using a_{z_τ} weights
7: **end for**
8: Determine $\mathscr{S}_{\text{win}}$ and payments
9: **for** each $u_i \in \mathscr{S}_{\text{win}}$ **do**
10: Compute $F_{\text{obs}}(d)$ and Chi-squared divergence from Benford's Law
11: **if** divergence $> \mu_{\text{UAV}}$ **then**
12: Dispatch UAV; forfeit deposit; blacklist
13: **end if**
14: **end for**
15: **for** each $u_i \in \mathscr{S}_{\text{win}}$ **do**
16: Update $P_{i,\tau+1}(c)$, $\psi_{i,\tau+1}$, and $\kappa_{i,\tau}$ based on m_i
17: Update $\bar{\mu}_{z_\tau}$ and N_{z_τ}
18: **end for**
19: **end for**
20: **return** $\mathscr{S}_{\text{win}}$, updated parameters, and adjusted deposits

4.4 Genetic Algorithm Design for Proactive Mobility Guidance

While the UUE-UCB mechanism primarily addresses privacy-preserving recruitment and quality-aware worker selection under bilateral location privacy constraints, spatial-temporal mismatch between learned worker profiles and dynamic task locations remains a challenge. To bridge this gap, we propose a TSGA that leverages priors accumulated from UUE-UCB including estimated sensing quality $\hat{m}_i$, task-type preference beliefs $P_{i,\tau}(T)$, and reliability-adjusted bid factors $\kappa_{i,\tau}$ as guided knowledge for proactive worker mobility.

Different from conventional genetic algorithms that treat mobility planning in isolation, TSGA's primary novelty lies in its UUE-UCB-informed initialization and adaptive repair mechanisms. These components embed worker-specific

knowledge directly into the evolutionary process, transforming standard search into a knowledge-driven optimization tailored to the PRIME framework.

Chromosome Encoding and Representation

TSGA adopts a real-valued task-sequence encoding. Each chromosome $\mathbf{g}_v$ consists of M genes, where the i-th gene $\text{Gene}_i = (gx'_i, gy'_i)$ denotes the recommended target grid for worker u_i. This representation maintains $O(M)$ space complexity and integrates directly with the selected worker set $\mathscr{S}_{\text{win}}$ and updated profiles from UUE-UCB.

UUE-UCB-Guided Population Initialization

The initial population is generated via a preference-and-quality-guided heuristic. Each worker u_i is biased toward high-value grids aligned with its UUE-UCB-learned task-type preference $P_{i,\tau}(T)$ and estimated quality $\hat{m}_i$, further weighted by the reliability factor $\kappa_{i,\tau}$. The remaining individuals are sampled uniformly within the feasible energy radius determined by E_i. This initialization narrows the search space and accelerates convergence by exploiting upstream learning outcomes.

Fitness Evaluation

The fitness function combines upstream estimates with system objectives:

$$f(\mathbf{g}_v) = \sum_{t_j \in \mathscr{T}} \sum_{u_i \in \mathscr{S}_\tau} \xi_{i,j} \Big(\hat{m}_i \cdot P_{i,\tau}(c_j) \Big) - \sum_{u_i \in \mathscr{S}_\tau} \Big(C_i(\Phi_\tau) + \lambda_e e_{\text{move},i} \Big), \tag{26}$$

where $\hat{m}_i$ and $P_i(T_j)$ are taken directly from the latest UUE-UCB updates. Hard constraint violations incur heavy terminal penalties.

Evolutionary Operators and Constraint Repair

TSGA applies elitism combined with tournament selection, arithmetic crossover on coordinate pairs, and adaptive Gaussian mutation with decaying variance across generations. After crossover and mutation, three adaptive repair operators enforce feasibility while preserving UUE-UCB priors: energy repair retracts the target coordinate toward the worker's current position with step size modulated by reliability score (gentler for more reliable workers); capacity repair redistributes excess workers to nearby grids prioritized by quality $\hat{m}_i$ and preference alignment; budget repair prunes lowest-Return on Investment(ROI) tasks based on marginal utility derived from UUE-UCB quality estimates.

TSGA terminates after a fixed number of generations or when fitness improvement falls below a threshold. By systematically embedding UUE-UCB priors into initialization, fitness evaluation, and repair, TSGA establishes a tightly coupled knowledge-transfer pipeline from privacy-preserving recruitment to dynamic mobility guidance. This integration constitutes the main contribution of the mobility component within PRIME: it exploits accumulated worker knowledge to achieve improved spatial matching and long-term utility under resource constraints.

The complexity of TSGA is governed mainly by its fitness evaluation. For each chromosome, evaluating M selected workers across $|\mathscr{T}|$ tasks takes $O(M \cdot |\mathscr{T}|)$. Other genetic operations (e.g., initialization, crossover, mutation) only require $O(M)$ per chromosome. For a population of size G evaluated over L generations, the fitness evaluation dominates the process, resulting in a final TSGA complexity of $O(L \cdot G \cdot M \cdot |\mathscr{T}|)$.

Based on the above analysis, the overall complexity of the PRIME framework sums the costs of SG-DCE, UUE-UCB, and TSGA. Retaining only the dominant terms, the total complexity simplifies to $O(T_r \cdot S \cdot n \cdot R_{\text{grid}}^2 + L \cdot G \cdot M \cdot |\mathscr{T}|)$. The first term accounts for the online privacy-preserving recruitment, while the second term represents the genetic-algorithm-based dynamic task allocation.

5 Performance Evaluation

5.1 Datasets and Settings

To evaluate the effectiveness of the proposed PRIME framework, we develop a real-map-based simulation dataset using an urban area of Qingdao, China. The selected region covers the latitude range of 36.05°–36.15° and the longitude range of 120.30°–120.45°, corresponding to an approximately 11.1 km × 13.5 km urban sensing area. The map is obtained from OpenStreetMap and discretized into a 200 × 200 grid, resulting in 40,000 spatial cells. This grid-based representation enables continuous worker mobility and task locations to be approximated within a discrete spatial domain.

In terms of experimental scale, the simulated Mobile Crowdsensing system contains 40–200 vehicular workers and 20–80 concurrent sensing tasks. Each task is further divided into 5–20 subtasks and requires 100–1000 MB of sensing data. Therefore, the number of sensing subtasks varies with the task scale, and the experimental setting covers both small-scale and relatively large-scale crowdsensing scenarios. Task requesters publish multi-capability sensing tasks at distinct spatial locations, and each task is associated with a capability requirement vector, data volume, and AoI constraint.

All experiments are implemented in MATLAB R2023b on a workstation equipped with an Intel Core i7 CPU and 32 GB RAM. Each experiment is repeated 50 times with different random seeds, and the reported results correspond to the average values.

We simulate a heterogeneous Mobile Crowdsensing system with dynamic task requesters and vehicular workers. Workers are characterized by heterogeneous capability vectors, sensing ranges, and execution costs, all normalized within $[0.1, 1]$. The number of preferred task types per worker, denoted by $|D_i|$, varies from 1 to 10 to reflect different participation preferences and engagement levels.

The system incorporates a collaborative edge computing architecture consisting of one cloud server and five base stations (BSs), each equipped with an edge server. The unit transmission delay from BS to cloud follows a Gaussian distribution $\mathscr{N}(1.5\,\mu\text{s/bit}, \sigma^2)$, where σ is set to $0.3\,\mu\text{s/bit}$.

Task arrivals follow a Poisson process with rate λ_t, and the maximum harvested green energy $E_n^{\text{green,max}}(t)$ at each edge server is also modeled as a Poisson process to capture temporal variability.

To emulate sensing uncertainty, ground-truth data is perturbed by additive noise. For trustworthy workers, the relative

error is uniformly distributed in $(0,5\%]$, while for untrustworthy workers, it follows a uniform distribution in $(10\%,50\%]$. This setup allows us to evaluate the robustness of the proposed mechanism against unreliable or malicious data submissions.

Default parameter values, distributions, and ranges for key variables—including network scale, capability vectors $\mathbf{r}_j$, edge server constraints such as channel capacity k and maximum CPU frequency $f_n^{\max}$, and algorithmic hyperparameters—are summarized in Table 2. This configuration ensures consistency across all compared methods.

Table 2: Key Simulation Parameters

Notation	Description
W	Worker pool size (40–200)
T	Number of concurrent tasks (20–80)
B	Platform budget (40000–80000)
R_i	Worker sensing radius (5–10 m)
$\lvert\mathbf{c}_i\rvert$	Number of worker capability types (1–3)
$\lvert\mathbf{r}_j\rvert$	Number of required task capabilities (5–7)
sv_i	Data sensing/processing rate (1–10 MB/s)
mv_i	Moving speed (1–5 m/s)
E_i	Energy budget (5000–6000)
Γ_i	Time budget (60–600 s)
DB_j	Required data volume (100–1000 MB)
k_c	Base cost coefficient (10)
q_j	Number of subtasks (5–20)
A_j	AoI threshold (10–60 s)
α_i	Movement energy coefficient (10^{-6}–10^{-5} J/m)
β_i	Sensing energy coefficient (10^{-4}–10^{-3} J/MB)
m_i	Ground-truth sensing quality ($\mathcal{N}(8,2)$)
ε	Differential privacy budget (0.1–1.0)
σ	UCB exploration coefficient ($\{10^{-2},10^{-1},1,10\}$)
$\hat{\gamma}_i$	Initial trust value (0.5)
ρ_{ij}	Normalized collateral ratio ($[0,0.2]$)
λ	Collateral incentive weight (0.1–1.0)
P	GA population size (20–100)
p_m	GA mutation probability (0.01–0.1)
p_c	GA crossover probability (0.6–0.9)
w_1, w_2	Utility weights (quality, freshness; tuned)
k	Effective switched capacitance (10^{-28})
$f_n^{\max}$	Maximum CPU frequency (1–3 GHz)

5.2 Baselines

To comprehensively evaluate the performance of the proposed PRIME framework, we select the following representative baseline methods:

- **Random Selection**: Workers are chosen uniformly at random in each round, without using any historical or quality information (serves as the simplest lower bound).
- **QLP-DCS-Based Selection**: We adopt the quality-aware budget-limited participant selection method proposed in QLP-DCS [7]. This method selects workers by optimizing the trade-off between sensing quality and budget consumption, typically using a quality-to-cost ratio under budget constraints. It serves as a representative heuristic baseline for cost-efficient participant selection in Mobile Crowdsensing systems.
- **Greedy**: Workers are ranked by a composite score (e.g., quality per cost or distance-adjusted bid) and the top-K are selected greedily (represents the most common heuristic in practical crowdsensing systems).
- **Q-BLPP**: We adopt the Quality-Enabled Bilateral Location Privacy-Preserving Service Construction Scheme proposed in Q-BLPP [12]. This scheme simultaneously protects the location privacy of both workers and the platform in mobile crowdsensing through differential privacy mechanisms and quality-aware task allocation, achieving a balanced privacy-quality trade-off. It serves as a strong privacy-aware baseline to assess PRIME's advantages in bilateral privacy protection strength, privacy-utility tradeoff, and overall system performance.

5.2.1 Evaluation Metrics

The following key metrics are adopted to evaluate system performance:

- **Cumulative Regret**: The accumulated performance gap with respect to the Oracle-Optimal strategy:

$$R(T)=\sum_{t=1}^{T}(\mu^*-\mu_{z_t}), \tag{27}$$

  which measures the long-term learning efficiency of the proposed mechanism.
- **Task Completion Rate (TCR)**: The ratio of successfully completed tasks within their AoI deadlines to the total number of tasks.
- **Mean Relative Error (MRE)**: The average relative deviation between estimated and ground-truth sensing values:

$$\mathrm{MRE}=\frac{1}{N}\sum_{j=1}^{N}\frac{|\hat{x}_j-x_j|}{x_j}, \tag{28}$$

  which evaluates the accuracy of truth discovery and reliability estimation.

5.3 Results and Discussion

Figure 3 compares system utility across all schemes over time. PRIME achieves the highest utility throughout, followed by Q-BLPP. Although Q-BLPP accounts for mutual privacy and sensing quality, it optimizes individual worker and task pairs independently, lacking joint exploration of multi-subtask combinations; this limits its performance under complex dynamic constraints. QLP-DCS and Greedy-Score attain only local improvements and are susceptible to resource misallocation under tight budget and coverage requirements. Random selection yields the lowest utility, as it ignores quality and spatial information entirely. PRIME addresses these limitations by coupling UUE-UCB's dual-track exploration and exploitation with TSGA's global multi-dimensional optimization, producing consistently superior task and worker alignment across all rounds.

Figure 4 and Figure 5 show that cumulative regret and MRE of quality estimation both decrease monotonically with the number of interaction rounds for all schemes, confirming that online learning improves allocation quality over time. PRIME attains the lowest regret and MRE, attributed to the joint effect of Benford's Law detection and dynamic deposit

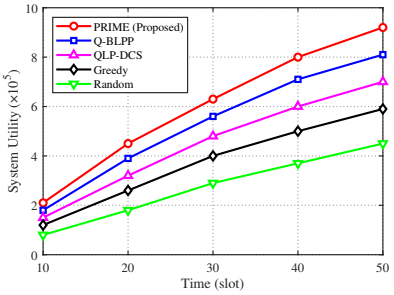

Figure 3: System Utility gain under Time.

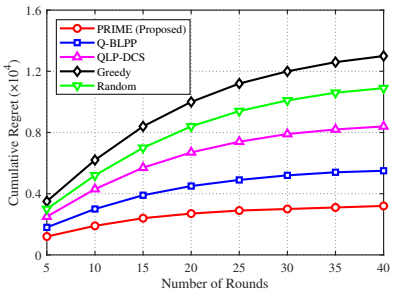

Figure 4: Cumulative Regret under Number of Rounds.

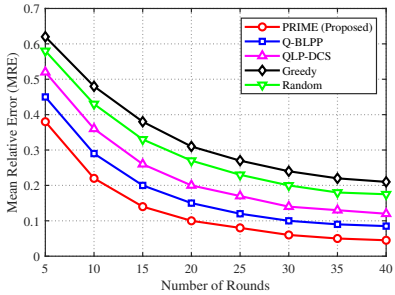

Figure 5: Mean Relative Error (MRE) under Number of Rounds.

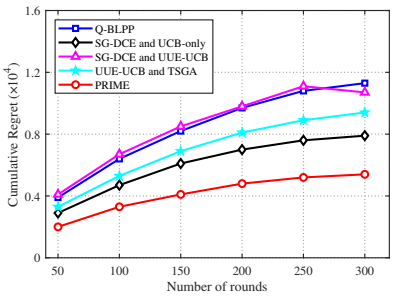

Figure 6: Ablation Study: Cumulative regret across different PRIME variants.

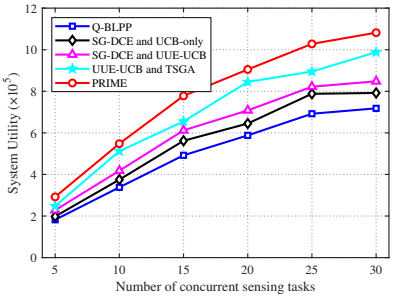

Figure 7: Ablation Study: System utility under varying task loads.

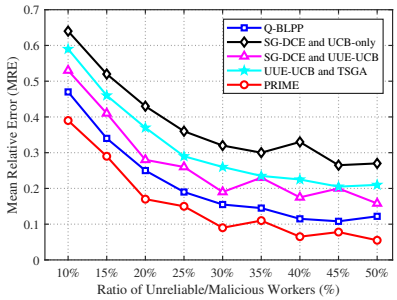

Figure 8: Ablation Study: Mean Relative Error (MRE) under different malicious worker ratios.

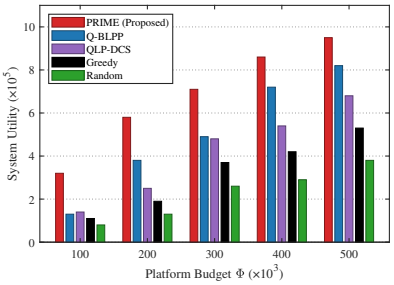

Figure 9: System Utility under different Budget.

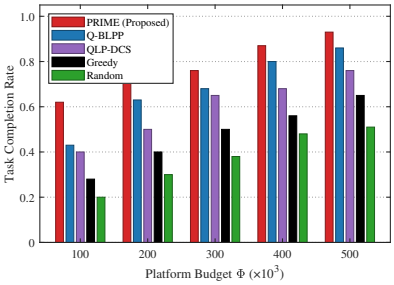

Figure 10: Task Completion Rate under different Budget.

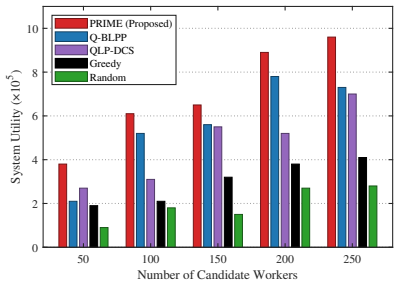

Figure 11: System Utility under different Number of Workers.

adjustment (ρ_{ij}, $\hat{\gamma}_i$), which suppress fraudulent submissions and stabilize the quality estimate $\hat{m}_i$ even under privacy-induced observation noise. Greedy-Score exhibits the slowest convergence, as it lacks a reputation feedback loop and accumulates estimation error from unfiltered noisy submissions.

5.4 Ablation Studies and Algorithmic Comparisons

The long-term learning efficiency of the proposed framework is first validated via the cumulative regret trajectories plotted in Figure 6, where the full PRIME framework converges to a sublinear regret of 0.54×10^4, representing an approximate 52% reduction over Q-BLPP (1.13×10^4). Isolating specific algorithmic features reveals that the standalone `PRIME_UCB` variant retains a superior learning trajectory (0.79×10^4) compared to the baseline, whereas removing the mobility layer (`PRIME_woTSGA`) or the security module (`PRIME_woDep`) significantly compromises convergence, raising terminal regrets to 1.07×10^4 and 0.94×10^4, respectively. The structural necessity of spatial-temporal coordination under varying task loads is quantified next in Figure 7. At the maximum density of 80 tasks, PRIME sustains the highest utility of 10.82×10^5, whereas the variant stripped of genetic sequence optimization (`SG-DCE and UUE-UCB`) drops sharply to 8.48×10^5; this performance gap validates that the knowledge-guided initialization and repair operators prevent allocation bottlenecks that hobble more basic combinations like `SG-DCE and UCB-only` (7.92×10^5) and `UUE-UCB and TSGA` (9.88×10^5). ly, Figure 8 evaluates adversarial resilience by tracking the Mean Relative Error (MRE) of quality estimation across a malicious worker ratio spanning 10% to 50%. PRIME exhibits excellent tracking precision, with its MRE declining from 0.39 to a terminal error of 0.055, demonstrating that the deposit-based economic deterrence continuously filters out deceptive data injections over successive interaction rounds. In contrast, ablation configurations lacking unified spatial-security coordination exhibit elevated error levels across the entire adversarial spectrum; the `SG-DCE and UCB-only` baseline plateaus with an MRE range of 0.64 to 0.27, while `UUE-UCB and TSGA` (0.21), `SG-DCE and UUE-UCB` (0.158), and the advanced `Q-BLPP` (0.122) fail to match the estimation stability of the integrated architecture.

5.5 Impact of Parameters

5.5.1 Impact of Platform Budget

Figure 9 and Figure 10 show system utility and TCR as functions of the platform budget Φ_t. Both metrics increase monotonically with Φ_t, as a larger budget expands the number of feasible recruitment rounds, broadens UUE-UCB's exploration of unknown workers, and accumulates richer historical feedback on sensing quality $\hat{m}_i$ and preference beliefs $P_{i,\tau}(\Gamma)$. This reduces information asymmetry in early rounds and improves subsequent task–worker alignment. Greedy-Score and Random Selection exhibit diminishing marginal gains because they cannot exploit accumulated feedback: additional budget is increasingly wasted on low-quality or previously rejected workers. PRIME feeds matching outcomes back into UUE-UCB and applies TSGA's ROI-aware repair to prune low-return task sequences, maintaining high budget utilization across all Φ_t values.

5.5.2 Impact of Number of Workers

Figure 11 and Figure 12 illustrate system utility and TCR as functions of worker pool size W. System utility rises with W because a larger candidate set increases the probability of identifying workers with high sensing quality $\hat{m}_i$, matched capability vectors $\mathbf{c}_i$, and low execution cost, thereby improving task coverage. TCR, however, declines as W grows under fixed budget Φ_t and task load T: intensified competition leaves more unknown workers unassigned, and the expanded pool amplifies information asymmetry during early exploration rounds, making it harder for UUE-UCB to build reliable quality estimates within a bounded number of interactions. PRIME mitigates this tension through UUE-UCB's preference-prior initialization and TSGA's global optimization, which together identify the high-value worker subset even as W scales, sustaining utility growth while limiting TCR degradation relative to the baselines.

5.5.3 Impact of Number of Tasks

Figure 13 and Figure 14 show that increasing task load T raises system utility but reduces TCR. A larger task set diversifies sensing demand, enabling the platform to better exploit worker capability heterogeneity $\mathbf{c}_i$ and extract higher cumulative value. TCR declines because fixed W and Φ_t cannot provide sufficient coverage for all requests; the platform is therefore forced to allocate resources to high-value tasks, leaving geographically isolated or low-return tasks unserved. PRIME's TSGA component prioritizes high-ROI task sequences and guides proactive worker mobility, achieving the best utility–coverage tradeoff among all evaluated schemes.

5.5.4 Impact of Worker Preferences and AoI Constraints

Figure 15 and Figure 16 examine the effect of reward sensitivity, defined as the degree to which workers preferentially bid on high-payment tasks. High sensitivity concentrates bids on lucrative tasks, intensifying local competition and causing spatial mismatch that leaves low-budget tasks unassigned. Greedy-Score is most vulnerable, as local score maximization accelerates budget depletion without global rebalancing. PRIME counteracts this via UUE-UCB's bid-adjustment factor $\kappa_{i,\tau}$ and TSGA's preference-aware sequence construction, which reallocate recruitment pressure across the task set and preserve overall cost-effectiveness.

Figure 17 and Figure 18 show the corresponding utility curves examine AoI sensitivity. Tighter AoI thresholds shrink the feasible mobility radius for each worker, reducing the number of valid task–worker pairs and lowering TCR across all schemes. PRIME incorporates AoI violation penalties directly into the TSGA fitness function and uses the energy-aware repair operator to enforce temporal feasibility, sustaining a higher TCR than Random Selection and Greedy-Score under the strictest AoI budgets.

5.5.5 Impact of Normalized Collateral Ratio

Figure 19 and Figure 20 show the effect of the normalized collateral ratio ρ_{ij} on system utility and task completion rate. As the normalized collateral ratio increases, untrustworthy workers face a higher risk of deposit forfeiture upon submitting falsified or low-quality data, which progressively filters them from the bidding pool without explicit platform intervention.

The resulting reduction in malicious participation lowers noise in quality estimation, allowing UUE-UCB to converge more rapidly toward reliable workers and allocate the platform budget Φ_t more precisely. Consequently, both system utility and TCR increase monotonically with the collateral ratio across all evaluated schemes.

The improvement is most pronounced for PRIME. Because PRIME couples the collateral-aware incentive mechanism directly with the UUE-UCB reliability score $\hat{\gamma}_i$ and the TSGA fitness function (Equation 26), a cleaner candidate pool immediately translates into more accurate preference alignment and higher-quality task sequences.

Baseline methods such as Greedy-Score and ε-Greedy also benefit from the reduced estimation noise, yet their gains plateau earlier due to the absence of a global optimization stage. Without TSGA's constraint-aware repair mechanism, the budget allocated to marginal workers cannot be effectively redistributed toward high-ROI task sequences.

Random selection exhibits the lowest sensitivity to the collateral ratio since it does not utilize worker quality information regardless of candidate pool purity.

These results demonstrate that the proposed collateral-aware deterrence mechanism acts as a self-regulating filtering process. By suppressing malicious participation during the early exploration phase, it reduces the learning burden of UUE-UCB and further amplifies the downstream optimization gains brought by TSGA-guided mobility, ultimately yielding a compounding improvement in long-term system performance.

Summary: Across all parameter dimensions (including platform budget, worker pool size, task load, reward sensitivity, Age-of-Information constraints, and collateral ratio), PRIME consistently outperforms the four baseline approaches in terms of both system utility and task completion rate. The results establish that UUE-UCB and TSGA is essential for achieving robust, cost-effective crowdsensing under bilateral location privacy and dynamic resource constraints.

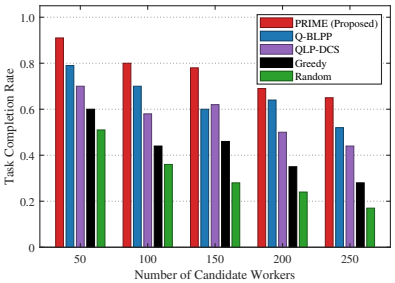

Figure 12: Task Completion Rate under different Number of Workers.

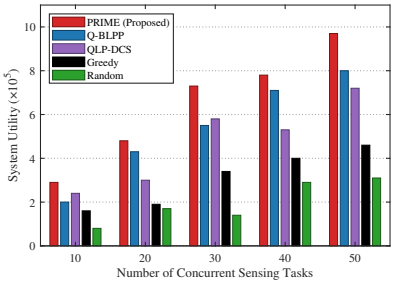

Figure 13: System Utility under different Number of Tasks.

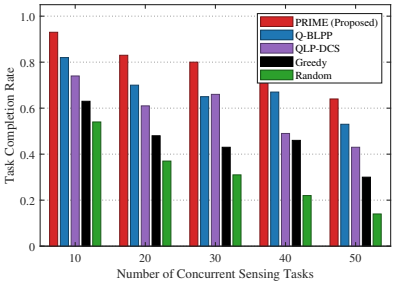

Figure 14: Task Completion Rate under different Number of Tasks.

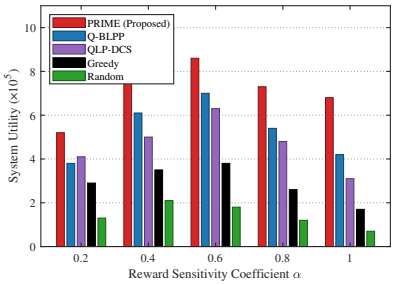

Figure 15: System Utility under different Reward Sensitivity.

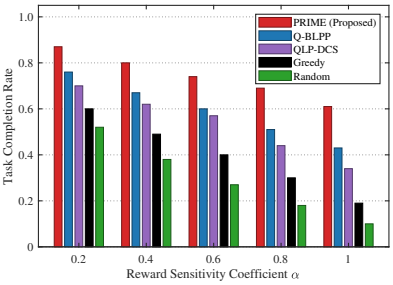

Figure 16: Task Completion Rate under different Reward Sensitivity.

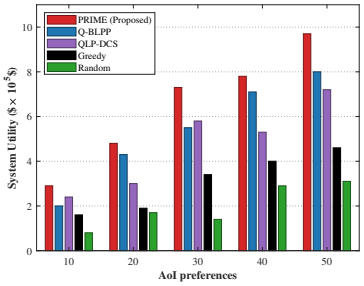

Figure 17: System Utility under different Number of Tasks (AoI constrained).

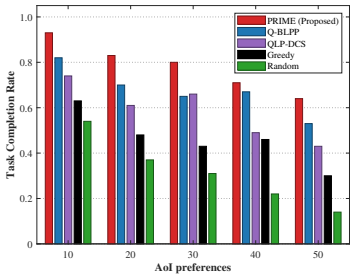

Figure 18: Task Completion Rate under different Number of Tasks (AoI constrained).

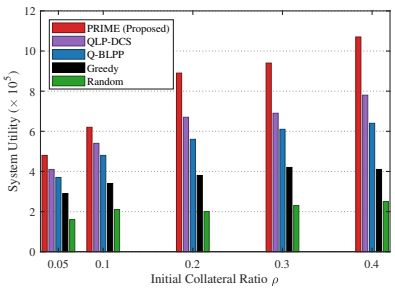

Figure 19: System Utility under different Collateral Settings.

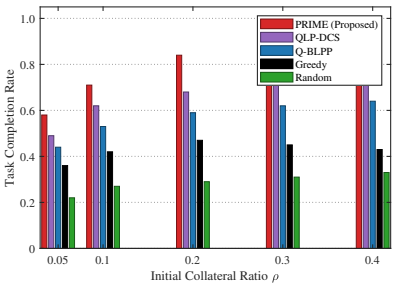

Figure 20: Task Completion Rate under different Collateral Settings.

6 Conclusion

This paper proposed the PRIME framework to jointly address bilateral location privacy, worker quality uncertainty, and spatial-temporal mismatch in heterogeneous mobile crowdsensing. Three tightly coupled components were developed: SG-DCE establishes mutual location privacy via grid-partitioned HMAC tokens; UUE-UCB balances worker exploration and exploitation through a dual-track bandit model augmented with Benford's Law detection and deposit-based penalty (ρ_{ij}, $\hat{\gamma}_i$); and TSGA transfers the accumulated quality priors ($\hat{m}_i$, $\kappa_{i,\tau}$) into preference-guided evolutionary optimization under energy, budget Φ_t, and AoI constraints. Simulation results across six parameter dimensions confirm that PRIME consistently achieves higher system utility, lower cumulative regret, and higher TCR than the considered baselines. Future work will extend UUE-UCB toward a federated worker profiling architecture and relax the single-platform assumption to admit multi-platform game-theoretic settings.

Funding

This work is supported by the Key Research and Development Program of Quzhou, China, No. 2025K132.

Author Contributions

Conceptualization, Haozhou Liu and Honglong Chen; methodology, Haozhou Liu, Honglong Chen and Huansheng Xue; software, Haozhou Liu, Huansheng Xue and Yongji Sun; validation, Haozhou Liu; formal analysis, Haozhou Liu; investigation, Haozhou Liu, Huansheng Xue, Yongji Sun and Junru Hei; resources, Honglong Chen and Yudi Guo; data curation, Haozhou Liu and Yongji Sun; writing—original draft preparation, Haozhou Liu; writing—review and editing, Haozhou Liu, Honglong Chen and Huansheng Xue; visualization, Haozhou Liu; supervision, Honglong Chen and Yudi Guo; project administration, Honglong Chen; funding acquisition, Honglong Chen. All authors have read and agreed to the published version of the manuscript.

Conflict of Interest

All the authors declare that they have no conflict of interest.

References

[1] Sun, P., Wang, Z., Wu, L., Feng, Y., Pang, X., Qi, H., Wang, Z.: Towards Personalized Privacy-Preserving Incentive for Truth Discovery in Mobile Crowdsensing Systems. IEEE Transactions on Mobile Computing **21**(1), 352–365 (2022). https://doi.org/10.1109/TMC.2020.3003673

[2] Liang, L., Fang, F., Zhang, P., Jia, Y., Wen, W.: A Two-Stage Privacy Preservation Framework for Untrusted Platforms in Mobile Crowdsensing. IEEE Transactions on Vehicular Technology **74**(4), 6586–6598 (2025). https://doi.org/10.1109/TVT.2024.3517747

[3] Lu, Y., Wang, X., Hawbani, A., Liu, P., Zhao, L., Liu, Z.: EHTA: An Environment-Cost-Based Heterogeneous Task Allocation in Vehicular Crowdsensing. IEEE Transactions on Mobile Computing **23**(12), 11535–11548 (2024). https://doi.org/10.1109/TMC.2024.3396512

[4] Liu, X., Chen, H., Lin, K., Li, Z., Chen, N., Sun, P., Wu, L.: THUS: A Two-Phase Cross-Platform Hybrid User Recruitment Strategy in Mobile Crowdsensing. IEEE Internet of Things Journal **13**(8), 17658–17670 (2026). https://doi.org/10.1109/JIOT.2026.3663224

[5] You, W., Peng, T., Xie, Z., Wang, G., Meng, W., Liu, Q., Luo, E.: Online Task Allocation Based on Lyapunov Optimization and Fuzzy Control System in Vehicular Mobile Crowdsensing. IEEE Transactions on Vehicular Technology **74**(11), 17123–17135 (2025). https://doi.org/10.1109/TVT.2025.3579642

[6] Yu, H., Li, P., Huang, W., Du, R., Xu, Q., Nie, L., Bao, H., Liu, Q.: Social-Aware Incentive Mechanism for Data Quality in Mobile Crowdsensing: A Three-Stage Stackelberg Game Approach. IEEE Internet of Things Journal **12**(7), 7980–7994 (2025). https://doi.org/10.1109/JIOT.2025.3531125

[7] Huang, Y., Guo, J., Yang, S., Liu, J., Liu, A., Tang, J., Wang, T., Dong, M., Song, H.: QLP-DCS: A Quality-Aware, Low-Cost, and Privacy-Preserving Data Collection Service for Mobile Crowd Sensing. IEEE Transactions on Services Computing **18**(4), 2326–2341 (2025). https://doi.org/10.1109/TSC.2025.3565374

[8] Zhao, B., Guo, W., Tian, B., Qiao, C., Pei, Q., Liu, X.: RATE: Privacy-Preserving Task Assignment With Bi-Objective Optimization for Mobile Crowdsensing. IEEE Transactions on Mobile Computing **23**(12), 13851–13865 (2024). https://doi.org/10.1109/TMC.2024.3439584

[9] Sun, Y., Chen, H., Xue, H., Hei, J., Lin, K., Yu, J.: Toward Location Privacy-Preserving Crowdsensing: A Secure Sorting Approach. IEEE Internet of Things Journal **13**(1), 1622–1633 (2026). https://doi.org/10.1109/JIOT.2025.3630835

[10] Wang, H., Yang, Y., Wang, E., Liu, W., Xu, Y., Wu, J.: Truthful User Recruitment for Cooperative Crowdsensing Task: A Combinatorial Multi-Armed Bandit Approach. IEEE Transactions on Mobile Computing **22**(7), 4314–4331 (2023). https://doi.org/10.1109/TMC.2022.3153451

[11] An, J., Ren, Y., Li, X., Zhang, M., Luo, B., Miao, Y., Liu, X., Deng, R.H.: Privacy-Preserving User Recruitment With Sensing Quality Evaluation in Mobile Crowdsensing. IEEE Transactions on Dependable and Secure Computing **22**(1), 787–803 (2025). https://doi.org/10.1109/TDSC.2024.3418869

[12] Tang, J., Cai, Y., Long, S., Shen, Y., Fan, K., Li, Z., Deng, Q., Liu, A.: Q-BLPP: A Quality-Enabled Bilateral Location Privacy-Preserving Service Construction Scheme in Mobile Crowd Sensing. IEEE Transactions on Services Computing **17**(6), 4151–4165 (2024). https://doi.org/10.1109/TSC.2024.3394690

[13] Xu, Y., Xiao, M., Zhu, Y., Wu, J., Zhang, S., Zhou, J.: AoI-Guaranteed Incentive Mechanism for Mobile Crowdsensing With Freshness Concerns. IEEE Transactions on Mobile Computing **23**(5), 4107–4125 (2024). https://doi.org/10.1109/TMC.2023.3285779

[14] Huang, Y., Chen, H., Ma, G., Lin, K., Ni, Z., Yan, N., Wang, Z.: OPAT: Optimized Allocation of Time-Dependent Tasks for Mobile Crowdsensing. IEEE Transactions on Industrial Informatics **18**(4), 2476–2485 (2022). https://doi.org/10.1109/TII.2021.3094527

[15] Ma, G., Chen, H., Huang, Y., Wei, W., Liu, X., Wang, Z.: Utility-Based Heterogeneous User Recruitment of Multitask in Mobile Crowdsensing. IEEE Internet of Things Journal **10**(11), 9796–9808 (2023). https://doi.org/10.1109/JIOT.2023.3236679

[16] Liu, J., Dong, S., Wen, J., Tang, B., Yu, Y.: TBSCrowd: A Blockchain-Assisted Privacy-Preserving Mobile Crowdsourcing Scheme From Threshold Blind Signatures. IEEE Internet of Things Journal **11**(11), 19344–19354 (2024). https://doi.org/10.1109/JIOT.2023.3342092

[17] Zhu, Y., Liu, A., Xiong, N.N., Dong, H., Zhang, S.: RPPS-TDC: Reputation and Privacy-Preserving Services Based Truth Data Collection for Blockchain-Enabled Crowdsensing. IEEE Transactions on Services Computing **17**(6), 4239–4253 (2024). https://doi.org/10.1109/TSC.2024.3470320

[18] Bai, J., Gui, J., Wang, T., Song, H., Liu, A., Xiong, N.N.: ETBP-TD: An Efficient and Trusted Bilateral Privacy-Preserving Truth Discovery Scheme for Mobile

Crowdsensing. IEEE Transactions on Mobile Computing **24**(3), 2203–2219 (2025). https://doi.org/10.1109/TMC.2024.3489717

[19] Xu, C., Song, W.: Intelligent Task Allocation for Mobile Crowdsensing With Graph Attention Network and Deep Reinforcement Learning. IEEE Transactions on Network Science and Engineering **10**(2), 1032–1048 (2023). https://doi.org/10.1109/TNSE.2022.3226422

[20] Hu, Y., Wang, J., Wu, B., Helal, S.: RL-Recruiter+: Mobility-Predictability-Aware Participant Selection Learning for From-Scratch Mobile Crowdsensing. IEEE Transactions on Mobile Computing **21**(12), 4555–4568 (2022). https://doi.org/10.1109/TMC.2021.3077636

[21] Xu, Y., Wang, Y., Ma, J., Jin, Q.: PSARE: A RL-Based Online Participant Selection Scheme Incorporating Area Coverage Ratio and Degree in Mobile Crowdsensing. IEEE Transactions on Vehicular Technology **71**(10), 10923–10933 (2022). https://doi.org/10.1109/TVT.2022.3183607

[22] Song, H., Li, P., Du, R., Yu, H., Huang, W., Nie, L., Bao, H., Liu, Q.: Unknown Task Selection and Worker Recruitment Using Two-Stage Multiarmed Bandit in Crowdsensing. IEEE Internet of Things Journal **12**(13), 24441–24456 (2025). https://doi.org/10.1109/JIOT.2025.3555013

[23] Ouyang, Y., Zeng, F., Xiong, N.N., Liu, A., Pedrycz, W.: MWRS: A MAB-Based Worker Recruitment Scheme With Tripartite Stackelberg Game for Reliable Mobile Crowdsensing. IEEE Transactions on Mobile Computing **24**(7), 5665–5680 (2025). https://doi.org/10.1109/TMC.2025.3535567

[24] Xiao, M., Wu, J., Huang, L., Wang, Y., Liu, C.: Multi-task assignment for crowdsensing in mobile social networks. In 2015 IEEE Conference on Computer Communications (INFOCOM), pp. 2227–2235 (2015). https://doi.org/10.1109/INFOCOM.2015.7218609

[25] Hu, T., Xiao, M., Hu, C., Gao, G., Wang, B.: A QoS-sensitive Task Assignment Algorithm for Mobile Crowdsensing. Pervasive and Mobile Computing **41**, 333–342 (2017). https://doi.org/10.1016/j.pmcj.2017.01.005

[26] Wang, J., Wang, F., Wang, Y., Wang, L., Qiu, Z., Zhang, D., Guo, B., Lv, Q.: HyTasker: Hybrid Task Allocation in Mobile Crowd Sensing. IEEE Transactions on Mobile Computing **19**(3), 598–611 (2020). https://doi.org/10.1109/TMC.2019.2898950

[27] Liu, K., Peng, S., Gong, W., Zhang, B., Li, C.: Hybrid User-Based Task Assignment for Mobile Crowdsensing: Problem and Algorithm. IEEE Internet of Things Journal **11**(11), 19589–19601 (2024). https://doi.org/10.1109/JIOT.2024.3367958

[28] Qi, H., Liwang, M., Hosseinalipour, S., Xia, X., Cheng, Z., Wang, X., Jiao, Z.: Matching-Based Hybrid Service Trading for Task Assignment Over Dynamic Mobile Crowdsensing Networks. IEEE Transactions on Services Computing **17**(5), 2597–2612 (2024). https://doi.org/10.1109/TSC.2023.3333832

[29] Qi, H., Liwang, M., Wang, X., Fu, L., Hong, Y., Li, L., Cheng, Z.: Accelerating Stable Matching Between Workers and Spatial-Temporal Tasks for Dynamic MCS: A Stagewise Service Trading Approach. IEEE Transactions on Mobile Computing **25**(2), 2878–2894 (2026). https://doi.org/10.1109/TMC.2025.3610915

[30] Wang, H., Liu, A., Xiong, N.N., Zhang, S., Wang, T.: TVD-RA: A Truthful Data Value Discovery-Based Reverse Auction Incentive System for Mobile Crowdsensing. IEEE Internet of Things Journal **11**(4), 5826–5839 (2024). https://doi.org/10.1109/JIOT.2023.3308072

[31] Zhang, J., Yang, X., Chen, P., Wang, Z., Li, W., He, Z., Li, K.: A Utility-Optimal Reverse Posted Pricing Mechanism for Online Mobile Crowdsensing Task Allocation. IEEE Transactions on Services Computing **18**(5), 2588–2601 (2025). https://doi.org/10.1109/TSC.2025.3592426

[32] Ji, G., Zhang, B., Zhang, G., Li, C.: Online Incentive Mechanisms for Socially-Aware and Socially-Unaware Mobile Crowdsensing. IEEE Transactions on Mobile Computing **23**(5), 6227–6242 (2024). https://doi.org/10.1109/TMC.2023.3321701